FIB Generated Antimony Nanowires as Chemical Sensors

Alois Lugstein*, Christoph Schoendorfer*, Youn-Joo Hyun*, Lothar Bischoff**, Philipp M. Nellen***, Victor Callegari***, Peter Pongratz****, and Emmerich Bertagnolli*

* Vienna University of Technology, Institute for Solid State Electronics, 1040 Vienna, Austria
** Research Center Dresden-Rossendorf Inc., POB 510119, D-01314 Dresden, Germany
*** EMPA, CH-8600 Dübendorf, Switzerland
****Vienna University of Technology, Institute for Solid State Physics, 1040 Vienna, Austria

ABSTRACT

Sb nanowires with a homogeneous distribution of diameters of about 25 nm and length up to several microns are synthesized by a FIB induced self-assembling process. We propose a model similar to the vapor-liquid-solid mechanism with Ga acting as catalyst. Thereby FIB processing produces mobile Ga species on the surface which rapidly agglomerate forming catalytic nanoclusters. Sputtered Sb diffuses on the surface and acts as a quasi-vapor phase source. When the solved Sb concentration exceeds saturation, nucleation sites will be formed which initiate the precipitation of the Sb. Individual nanowires transferred onto isolating substrates have been contacted by electron beam lithographically processed Ti/Au pads for electrical characterization. In the contrary to ambient of CO, He and H_2, where no influence is observed, the conductivity of the Sb nanowire is highly sensitive on water and ethanol and a resistivtiy change over 4 orders of magnitude was observed.

Keywords: nanowires, focused ion beam, humidity sensor, self assembling

I. INTRODUCTION

Low-dimensional nanostructures are usually fabricated using either a top down or a bottom up strategy. The former technique is extremely flexible, but suffers from limitations in minimum feature size and uniformity. The latter one, utilizing spontaneous self-ordering effects, is limited by the broad size distribution and the lack of control of the positioning of the self-organized nanostructures. In this context the discovery of the appearance of periodic structures with dimensions in the nanometer regime induced by ion bombardment has attracted growing interest due to the possibility of obtaining a self-organized formation of nanometer structures [1].

Appleton et al. found that heavy-ion implantation leads to the formation of craters with diameters of about 20nm due to morphological instabilities in the amorphous phase of initial crystalline Ge [2]. Wang and Birtcher observed the generation of sponge-like porous structures on Ge [3].

Nitta et al. [4] and Kluth et al. [5] reported the development of an anomalous cellular structure followed by the formation of a network of nanoscale rods on ion irradiated GaSb which is proposed to result from a defect formation mechanism based on movement of the point defects induced by ion implantation.

In this paper we propose a process very similar to the vapor-liquid-solid (VLS) mechanism in which various metals such as Au [6], Fe [7], or Ti [8] catalytically enhance the growth of nanowires. Our study differs from most of the previous reports on VLS grown nanowires in that an intense focused Ga ion beam initiates the growth of nanowires at room temperature without using any additional materials source.

II. EXPERIMENTAL

Thin lamellas of antimony samples with purity > 99.999% were prepared and cleaned by rinsing with acetone and isopropyl alcohol followed by blow-drying with pure nitrogen. The antimony with sufficient initial smoothness was exposed to a 50 keV focused ion beam (FIB) with a diameter of 70 nm and a beam current density of 0.8 A/cm^2. No gases were introduced into the high vacuum chamber and the sample was kept at room temperature. The topographical and compositional evolution of the Sb surfaces irradiated by FIB, is investigated by means of scanning electron microscopy (SEM), high resolution transmission electron micrsocopy (RTEM), selected area diffraction (SAD), and energy dispersive X-ray diffraction (EDX) measurements.

For the purpose of patterning the FIB is scanned over a predefined area in discrete steps with well-defined step size and dwell time, i.e. the time the beam remains on each single spot. Each scan across the selected area deposits an ion fluence which is correlated to the above mentioned parameters. Single pass milling denotes a scanning strategy where the desired ion fluence is deposited within one single scan. For multi pass milling, the beam is scanned several times across the predefined area and the total ion fluence is dependent on the number of scan repetitions of the FIB.

III. RESULTS AND DISCUSSION

Fig. 1a shows a SEM image of the Sb surface after multi pass milling of a (2x2)µm² wide box with a ion fluence of $6.2x10^{18}$ Ga ions/cm². The rim of the several micrometer deep hole is surrounded by a dense network of nanofibers which show very uniform diameters in the range of 25nm. Milling the same box with the same ion fluence in single pass mode leads to the formation of a pattern shown in Fig. 1b. Thereby the FIB scan starts in the upper left of the box and moves along in serpentines with a pixel and line spacing both of 10nm, which guarantees a nearly uniform ion fluence distribution (>99%) [18]. The whole FIB modified area is covered by nanofibers with the exception of the last line scan routed from the lower right to the lower left edge. Nanofibers reach even 2µm beyond the rim of the FIB milled area. Fig. 1c shows the Sb surface after single pass milling viewed under a tilt angle of 75°. The FIB generated nanowire extrusions do not form a plane porous disc as one could assume from the top view SEM image in Fig. 1b.

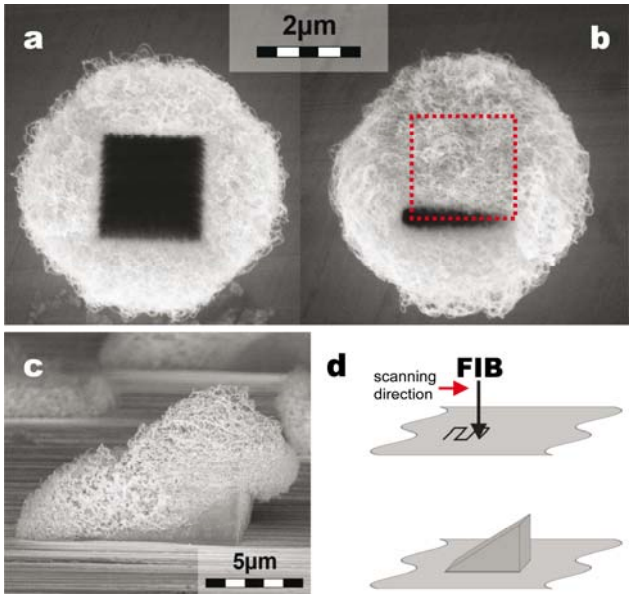

Figure 1: Sb surface processed using a 50keV Ga FIB with an ion current of 200pA. (2x2)µm² milling areas irradiated by an ion fluence of $6.2x10^{18}$ions/cm² in (a) multi pass mode and (b) single pass mode, tilted view SEM image of a (10x10)µm² milling area (c) exposed to an ion fluence of $3.1x10^{18}$ions/cm² processed in single pass mode, schematic sketch (d) visualizing the FIB scanning strategy and the resulting uplifted nanofiber network.

As shown in the schematic of Fig. 1d, the nanofibers appear on a ramp-like base normal to the plane rising along the scan direction of the FIB. The formation of this ramp-like structure is a result of the pixel-by-pixel and accordingly of the line-by-line scanning strategy. Scanning the first line of the predefined milling area leads to nanofiber growth even beyond the ion irradiated region.

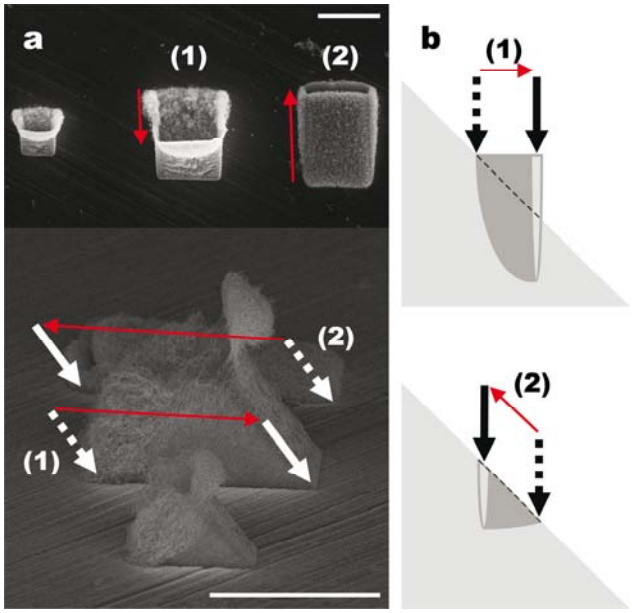

Figure 2: (a) SEM images of Sb surfaces milled under an angle of FIB incidence of 45°. The uppermost top view SEM image and the side view show the resultant pattern achieved under different scanning directions, which are indicated by the red arrows. Track (1) denotes a FIB guidance from higher to lower surface level on the tilted sample, track (2) denotes the opposite direction. The white arrows mark the incident direction of the FIB whereby the dotted arrows denote the start position of the scanning FIB beam. Scale bars, 10µm. (b) Principle sketch to point out the guidance of the FIB and the resulting structure formation.

By the guidance of the FIB through the subsequent lines, nanofibers which were grown on the not yet exposed part in the forefront of the scanning beam are removed by sputtering. Nanofibers in already irradiated zones, i.e. behind the scanning beam, remain unaffected. These nanofibers form a network which is further densified by redeposited Sb. Due to the ongoing FIB scanning this nanofiber network reduces the escape angle for the sputtered Sb and more and more of them are picked up by the network which leads to an upraising of the structures. Accordingly, FIB milling under oblique angles as schematically shown in Fig. 2b should lead to an increase or decrease of the uplifting effect due to the variation of the escape angles for sputtered Sb. The results obtained for FIB processing of a Sb surface tilted by 45° relative to the incident focused ion beam are shown in Fig. 2a. Depending on the scanning direction of the FIB the escape angles of the sputtered substrate material change. The scanning direction from higher to lower levels denoted as track (1) in the schematic of Fig. 2b (escape angle of 135°) results in an upraised structure. Hardly any uplifting can be observed when scanning in the opposite direction denoted as track (2) (escape angle 45°). The smaller (5x5)µm² FIB milled box

in Fig. 2a (the left box in the top view and the one in front of the side view image) shows the impact of the box length on this uplifting effect. The height of the uplifting increases with the length of the FIB milled box. For boxes with a length of 15µm or above this height levels out at about 10µm.

Extensive TEM, SAD and EDX of individual nanofibers prove that they are completely amorphous even in the nanometer scale and consist of pure antimony. The TEM image in Fig. 3a shows the exceptional uniform diameters of the nanofibers of about 25nm along their entire length.
The FIB modified samples covered by the nanofibers were annealed in a special furnace setup which allows processing at well-controlled temperature profiles in He atmosphere. Several experiments showed that the temperature ramp is a crucial parameter for the grain size of the resulting re-crystallized structure whereby the diameter and shape of the nanowires remain unaffected by the annealing. The HRTEM image in Fig. 3b displays a Sb nanowire after moderate thermal annealing at 453K for 30min. The diffraction pattern in Fig. 3c shows the most prominent (110) and (120) reflections for Sb with its trigonal crystal structure and the lattice parameter of 0,354nm is consistent with the tabulated value for bulk Sb. Fig. 3d shows the EDX spectrum of the investigated nanowire. The dashed lines mark energies for Ga in the EDX spectrum. As there the peaks for Ga are missing the nanowire seems to consist of pure Sb. The copper signal originates from the sample holder ring.
The observed nanofiber formation, even several microns aside the FIB irradiated surface can not be explained by point defect as proposed by Nitta et al. [9]. We propose a model similar to VLS with Ga acting as catalyst [10]. VLS deals with the fact that a catalytic metal particle on the sample surface - if the ambient temperature is high enough - forms a liquid alloy cluster and serves as the preferential site for adsorption of reactant from the vapor phase. It is supposed that supersaturation is the driving force for nucleation of seeds at the interface between alloy cluster and the substrate surface giving rise to a highly anisotropic growth of nanostructures. Nanowire growth from the base continues as long as the droplet remains in a liquid state and supersaturation is maintained.
At present, we do not understand the origin of the tangling of the nanowires although we note that extensive tangling has been observed previously in Ga based VLS processes [11]. The authors of also stated that Ga droplets could simultaneously catalyze the growth of hundreds of thousands of nanowires.

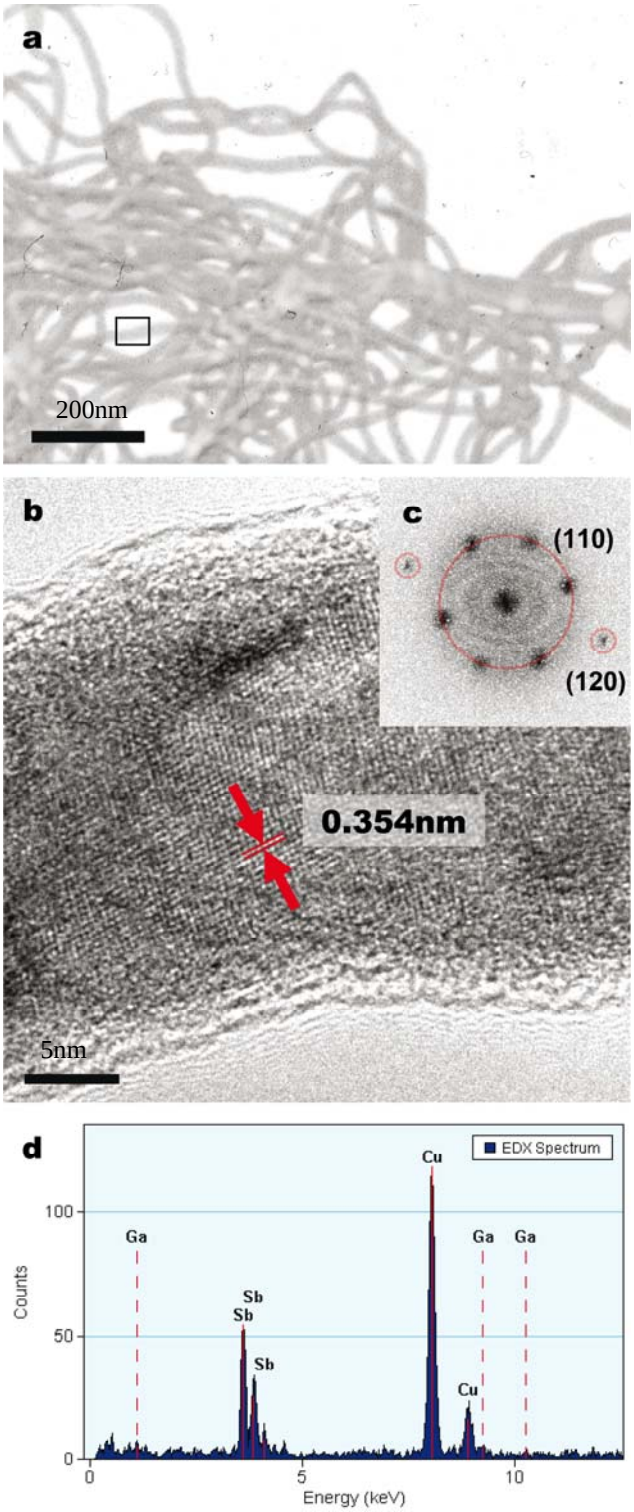

Figure 3: (a) low magnified TEM image. (b) HRTEM micrograph shows the part of a Sb nanofiber (marked by the rectangle in Fig. 3) after annealing at 453K. (c) diffraction pattern ((110) and (120) reflections) of the nanowires after the annealing. (d) EDX spectrum.

NSTI-Nanotech 2008, www.nsti.org, ISBN 978-1-4200-8505-1 Vol. 3

For electrical characterization the FIB generated nanowires are transferred onto isolating substrates. Individual nanowires are contacted with electrodes consisting of 3nm Ti (as an adhesion promoter) and 60nm Au, which is performed by means of electron beam lithography (EBL). During the measurements the ambient humidity showed a great impact on the current-voltage characteristic of a single Sb nanowire, which indicated the sensing potential of this device. Therefore the electrical measurements was performed under well-defined conditions. We investigated the sensing capability of single Sb nanowires for H_2, He, O_2, CO, H_2O and ethanol. To compare the impact of different gases and pressures the gas response or sensitivity of the nanowire sensor is defined as the ratio between Rg (the resistance when the sensor is exposed to a selected amount of gas) and R_0 (the resistance of the device in vacuum).

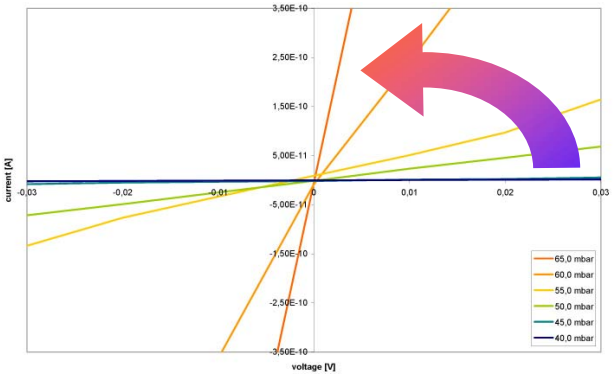

Figure 4: Evolution of the conductance of the Sb nanowire exposed to ethanol vapor.

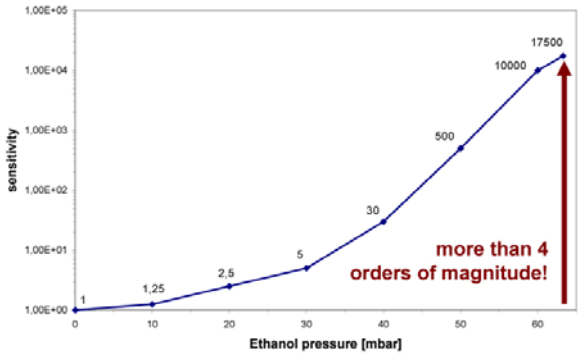

Figure 5: Sensitivity curve of the Sb nanowire sensor. From 0 to 100% saturation of ethanol vapor in the chamber the sensitivity changes by a factor of 17500. All measurements are carried out at room temperature (22°C).

Whereas no response was detected for H_2, He, O_2, and CO, a huge change in the conductance could be observed for ethanol and water. The curves displayed in Fig. 4 shows the current-voltage characteristics of a single Sb nanowire as a function of ethanol pressure. It is impressively shown that the conductance depends on the quantity of the gas to be detected. The graph in Fig. 5 gives an idea of the sensing potential of this Sb nanowire device as the sensitivity increases by more than four orders of magnitude depending on the introduced ethanol amount.

IV. SUMMARY

In summary, the FIB irradiation of Sb with 50keV Ga ions at room temperature leads to the formation of a porous network of pure Sb nanofibers. The as-grown nanofibers are amorphous with remarkable uniform diameters in the range of about 25nm along their entire length. Re-crystallization of the Sb nanofibers could be achieved by moderate thermal annealing at temperatures of about 473K. Depending on the temperature ramp and heating duration finely grained crystallites as well as single crystalline regions along the nanowires can be obtained.
Sensors realized from these Sb nanowires were very sensitive on water vapor and ethanol gas. The ethanol and water sensing are completely reversible processes, which temporarily enhance the electrical conductivity of the Sb nanowire.

V ACKNOWLEDGMENTS

This work is partly funded by the Austrian Science Fund (Project No. 18080-N07) and the Sixth EU Framework Program for Research and Technological Development (FP6) project "Charged Particle Nanotech" (CHARPAN).

REFERENCES

1 Z. X. Jiang, P. F. A. Alkemade, Appl. Phys. Lett. 73, 315 (1998); J. Erlebacher, M. J. Aziz, E. Chason, M. B. Sinclair, J. A. Floro, Phys. Rev. Lett. 82, 2330 (1999); S. Rusponi, G. Constantini, C. Boragno, U. Valbusa, hys. Rev. Lett. 81, 2735 (1998).
2 B. R. Appleton, O. W. Holland, D. B. Poker, J. Narayan, D. Fathy, Nucl. Instr. and Meth. in Phys. Res. B 7-8, 639 (1985).
3 L. M. Wang, R. C. Birtcher, Appl. Phys. Lett. 55, 2494 (1989); L. M. Wang, R. C. Birtcher, Phil. Mag. A 64, 1209 (1991).
4 N. Nitta, M. Taniwaki, Y. Hayashi, T. Yoshiie, J. Appl. Phys. 92, 1799 (2002).
5 S. M. Kluth, J. D. Fitz Gerald, M. C. Ridgway, Appl. Phys. Lett. 86, 131920 (2005).
6 . I. Persson, M. L. Larsson, S. Stenström, B. J. Ohlsson, L. Samuelson, L. R. Wallenberg, Nature 3, 677 (2004).
7 A. M. Morales, C. M. Lieber, Science 279, 208 (1998).
8 T. I. Kamins, R. S. Williams, Y. Cheng, Y. L. Chang, Y. A. Chang, Appl. Phys. Lett. 76, 562 (2000).
9 N. Nitta, M. Taniwaki, Y. Hayashi, T. Yoshiie, J. Appl. Phys. 92, 1799 (2002).
10 M. K. Sunkara, S. Sharma, R. Miranda, G. Lian, E. C. Dickey, Appl. Phys. Lett. 79, 1546 (2001).
11 Z. W. Pan, Z. R. Dai, C. Ma, Z. L. Wang, J. Am. Chem. Soc. 124, 1817 (2002).